



HAL
open science

Multi-faceted particle pumps drive carbon sequestration in the ocean

Philip W. Boyd, Hervé Claustre, Marina Lévy, David Siegel, Thomas Weber

► **To cite this version:**

Philip W. Boyd, Hervé Claustre, Marina Lévy, David Siegel, Thomas Weber. Multi-faceted particle pumps drive carbon sequestration in the ocean. *Nature*, 2019, 568 (7752), pp.327-335. 10.1038/s41586-019-1098-2 . hal-02117441

HAL Id: hal-02117441

<https://hal.science/hal-02117441>

Submitted on 27 Nov 2020

HAL is a multi-disciplinary open access archive for the deposit and dissemination of scientific research documents, whether they are published or not. The documents may come from teaching and research institutions in France or abroad, or from public or private research centers.

L'archive ouverte pluridisciplinaire **HAL**, est destinée au dépôt et à la diffusion de documents scientifiques de niveau recherche, publiés ou non, émanant des établissements d'enseignement et de recherche français ou étrangers, des laboratoires publics ou privés.

1 **Multi-faceted particle pumps drive carbon sequestration in the ocean**

2

3

4

Revised for Nature 10 January 2019

5

6

7 Philip W. Boyd¹ Hervé Claustre², Marina Levy³, David A. Siegel⁴, Thomas Weber⁵

8

9 ¹Institute for Marine and Antarctic Studies, University of Tasmania, Hobart, Tasmania,
10 Australia

11 ²Sorbonne Université & CNRS, Laboratoire d'Océanographie de Villefranche-sur-mer
12 (LOV), 06230 Villefranche-sur-Mer, France.

13 ³Sorbonne Université, LOCEAN-IPSL, CNRS/IRD/MNHN, 4 Place Jussieu, 75252 Paris
14 CEDEX 05, France.

15 ⁴Department of Geography & Earth Research Institute, University of California, Santa
16 Barbara, Santa Barbara, CA, 93106, USA,

17 ⁵Department of Earth and Environmental Sciences, University of Rochester, Rochester, NY
18 14627

19

20 **Orchid #**

21 **Philip Boyd <http://orcid.org/0000-0001-7850-1911>**

22 **Hervé Claustre 0000-0001-6243-0258**

23 **Marina Levy 0000-0003-2961-608X**

24 **David Siegel <https://orcid.org/0000-0003-1674-3055>**

25 **Thomas Weber 0000-0002-4445-6742**

26

27

28

29

30

31

32

33

34 **The ocean’s ability to sequester carbon out of contact with the atmosphere exerts an**
35 **important control on global climate. The biological pump drives carbon storage in the**
36 **deep ocean and is thought to function via gravitational settling of organic particles from**
37 **surface waters. However, the settling flux alone is often insufficient to balance**
38 **mesopelagic carbon budgets or meet the demands of subsurface biota. Here, we review**
39 **additional biological and physical mechanisms that inject suspended and sinking**
40 **particles to depth. Together, these “particle injection pumps” likely sequester as much**
41 **carbon as the gravitational pump, closing carbon budgets and motivating further**
42 **investigation of their environmental controls.**

43

44

45

46

47

48

49

50

51

52

53

54

55

56

57

58

59 **Introduction**

60 Open ocean waters store (sequester) carbon out of contact with the atmosphere on decadal to
61 millennial timescales, exerting a major control on global climate by regulating atmospheric
62 carbon dioxide partial pressure ($p\text{CO}_2$)¹. The magnitude of ocean carbon storage is governed
63 by two well-established mechanisms that maintain a surface-to-deep ocean gradient of
64 dissolved inorganic carbon (DIC) – the biological and the solubility pumps^{2,3}. The solubility
65 pump delivers cold, dense, DIC-rich waters to depth mostly at high latitudes, whereas the
66 biological pump globally exports particulate organic carbon (POC) from surface waters. POC
67 export is largely attributed to the gravitational settling of a subset of the particle assemblage^{1,4}
68 – a process we refer to as the “biological gravitational pump” (BGP).

69 The BGP is the key link between upper ocean photosynthetic carbon fixation, the sustenance
70 of mid-water biota, and carbon storage in the oceans’ interior^{4,5}, and is thought to account for
71 ~90% of the vertical DIC gradient, while the solubility pump explains the remainder¹. In the
72 absence of the BGP, models predict atmospheric $p\text{CO}_2$ would be higher by nearly twofold⁶.

73 Contemporary and paleoceanographic observations both reveal that carbon sequestration by
74 the BGP is affected by environmental changes in light, temperature, stratification and nutrient
75 availability^{7,8}, and can itself drive dramatic climate shifts such as glacial-interglacial cycles⁸.

76 Future climate projections suggest that the functioning of the BGP will be altered by ocean
77 global change^{7,9}, potentially feeding back on anthropogenic climate warming¹⁰. As a
78 consequence, quantification of its functioning requires a reliable baseline of accurate
79 measurements.

80 The underlying principles of the BGP are long established¹¹: organic particles are continually
81 produced and recycled in sunlit surface waters, and a small fraction of these settle into the

82 oceans' interior. The strength of the BGP is often quantified as the rate of particle "export"
83 from the euphotic zone, the surface mixed layer, or across an arbitrary horizon at 100m¹². As
84 they sink, particles undergo myriad transformations, which lead to pronounced vertical
85 attenuation of the particle flux that is often described as a power law relationship, referred to
86 as the "Martin Curve"¹³. The efficiency of the BGP is defined here as the time that exported
87 carbon is kept sequestered from the atmosphere within the ocean's interior. It is driven by the
88 depth scale of flux attenuation and pathways of ocean circulation that carry remineralized
89 carbon dioxide back to the surface¹⁴. Carbon is sequestered for timescales longer than a year
90 by particles that penetrate the permanent pycnocline (beneath the wintertime mixed layer)
91 and up to centuries by those that reach deep water masses (generally >1000m). Together, the
92 strength and efficiency of the BGP determine the total quantity of carbon sequestered
93 biologically in the ocean interior.

94 Recently, analyses of global and regional ocean carbon budgets have identified conspicuous
95 imbalances (i.e., two to three-fold less storage) when BGP export fluxes are compared with
96 those derived from geochemical tracers^{15,16}, highlighting the need to reassess the pathways
97 that contribute to carbon storage. Furthermore, rates of site-specific particle export appear to
98 be insufficient to meet the carbon demand of mid-water life (termed mesopelagic biota) by
99 two-to three-fold¹⁷⁻²⁰, but in one study can be balanced using community respiration¹⁸. There
100 is considerable debate over the reasons for these carbon deficits, ranging from biases inherent
101 in observational technologies^{17,21} to the potential role of other carbon (dissolved and/or
102 particulate) delivery mechanisms to deep waters^{16,22,23}. Traditionally, the biogeochemical
103 functioning of the BGP has been evaluated from quasi one-dimensional (1D) observations of
104 particle flux (Box 1), and extrapolated using Earth System Models (ESMs, parameterised
105 with observations²⁴⁻²⁶) and/or remote-sensing observations²⁶. This approach cannot capture

106 more complex mechanisms of carbon export that are highly variable in space and time (Box
107 1), potentially resulting in the reported carbon budget deficits.

108 Multiple lines of research have revealed the importance of additional export pathways,
109 physically (e.g. subduction) and/or biologically (e.g. large mesopelagic migrators) -mediated,
110 that inject particles to depth, termed here Particle Injection Pumps (PIPs)^{23,27-30}. These
111 mechanisms can potentially export all particle classes to depth, and thus challenge the
112 conventional view of gravitational sinking as the dominant downward pathway for particles
113 into the oceans' interior. The characteristics of PIPs fundamentally change our understanding
114 of biological carbon sequestration: first, PIPs can animate particle transport spatially into
115 three dimensions (3D), in contrast with the BGP where the vertical dimension is predominant
116 (1D); second, global estimates of PIP carbon fluxes are significant relative to those for the
117 BGP^{27,28}, and third, these mechanisms cannot be readily quantified using the traditional
118 toolbox applied to investigate the BGP (Box 1). Overall, the PIPs will increase the strength
119 of the biological pump beyond estimates based on gravitational flux alone, and can change its
120 efficiency by altering the depth of carbon export.

121 The fate of exported carbon following its delivery to depth has also proven more complex
122 and heterogeneous than previously recognized. Particle flux attenuation is now known to vary
123 systematically in space^{14,31,32} and time³³, suggesting the traditional empirical view¹³ must be
124 replaced by a mechanistic one that considers particle composition and architecture, microbial
125 metabolism, and transformation processes¹⁷.

126 Together, these developments stand to reshape our understanding of particle transport and
127 remineralisation in the oceans' interior. Here, for open ocean systems we review: the
128 mechanisms, rates, and depths of particle injection by each PIP; the potential for each
129 mechanism to close observed deficits in ocean carbon budgets; and the corresponding

130 remineralisation depths of exported POC in the deep ocean. We finish by outlining future
131 research directions needed to synthesize these developments into a new mechanistic, four-
132 dimensional (4D) view of carbon export and sequestration. The review does not detail the
133 important role of dissolved organic carbon subduction^{22,23}, nor cover the dark microbial
134 carbon pump³⁴ or chemolithotrophy³⁵ which have been reviewed elsewhere (S-Table 1).

135

136 **Particle injection pump mechanisms**

137 PIPs differ in their mechanisms, temporal-spatial scales (Fig. 1, Fig. 2a), and/or geographical
138 extent, but have common features: i) they can act on all particles from suspended to sinking
139 (Fig. 1); ii) they typically inject particles below the euphotic zone (i.e., the export depth for
140 the BGP), potentially reaching depths $>1000\text{m}$ ²⁸⁻³⁰ depending on the injection mechanism
141 (Fig. 1, Fig. 2b); iii) they occur concurrently with the BGP but cannot be measured with
142 techniques developed to quantify gravitational settling^{13,32} (Box 1); iv) their dynamic nature
143 (i.e., physical transport^{23,27,28} or patchiness of animal distributions³⁰) means that the interplay
144 between their vertical and horizontal vectors and temporal scales varies significantly (Fig. 1).
145 Hence, a 4D sampling framework is required to constrain them (Box 1). The main
146 characteristics of each PIP are elucidated below.

147 Particle export driven by physical subduction includes several processes driving the vertical
148 transport of near-surface particles that act on different space/time scales: subduction caused
149 by mixed-layer shallowing (termed the mixed-layer pump^{29,36}); subduction by large-scale
150 (100-1000 km) circulation (termed the large-scale subduction pump)²³; and subduction by
151 mesoscale (10-100 km) to submesoscale (1-10 km) frontal circulation (termed the eddy-
152 subduction pump^{23,27,28}).

153 Carbon export by the mixed-layer pump is driven by biological accumulation of particles
154 throughout the spring/summer growth season, which are then diluted to the depth of the
155 mixed layer during winter, and left in the oceans' interior during early spring stratification
156 (Box 1). This pump operates on wide-ranging time-scales from days/weeks³⁷ to seasons^{29,37},
157 predominantly in mid and high latitude regions characterised by strong seasonal variability in
158 mixed-layer depth (Fig. 2a). Although these concepts are long-established³⁶, only recently
159 have they been scrutinised in detail using advances in optical profiling (BGC-Argo) floats
160 and satellite particle proxies to track particle accumulation rates in relation to changes in
161 surface mixed-layer depth (Box 1).

162 The large-scale subduction pump is a 3D advective mechanism directed from the seasonal
163 mixed-layer into the oceans' interior, driven by Ekman pumping and horizontal circulation
164 across a sloping mixed-layer³⁸. Subduction rates were first estimated for the North Atlantic³⁹,
165 and then globally using data-assimilating models⁴⁰. The wide-ranging subduction rates (1-100
166 m/year)^{39,40} are small relative to BGP particle settling rates^{11,12}, but subduction occurs over
167 large regions of the global ocean boosting the magnitude of carbon delivery to depth.

168 The frontal-associated eddy-subduction pump subducts particle-rich surface waters on
169 timescales of days and across spatial scales of 1-10 km, driven by strong vertical circulation
170 associated with fronts and eddies^{27,28,41-44}. Gliders are now used to map 3D dynamic eddying
171 flow fields (Box 1), finding evidence for penetration of high particle stocks (co-located POC
172 and chlorophyll indicative of viable phytoplankton) from the spring bloom, conspicuous as
173 distinct filaments at 100-350 m depth at the eddy periphery²⁸ (Box 1). Mapping revealed the
174 co-location of high POC filaments and negative vorticity to depths near the permanent
175 pycnocline²⁸, and the mechanism is supported by high-resolution simulations in which eddy
176 subduction of particles is a recurring feature⁴⁵⁻⁴⁸. The strength of the eddy-subduction pump

177 is governed by the vigour and penetration of the vertical circulation, in conjunction with local
178 POC stocks over the frontal area^{27,49}. Eddy subduction rates span 1-100 m d⁻¹ (c.f. 20 to >
179 100 m d⁻¹ for the BGP^{11,12}) depending on the eddy or frontal structure. Modelling indicates
180 that these subducted particles are remineralised more rapidly (i.e., at relatively shallow depths)
181 relative to gravitationally-sinking particles²⁷.

182 The concept for the ‘mesopelagic migrant pump’ is based on long-established observations of
183 diurnal vertical migration⁵⁰ (Box 1). This pump extends the remineralisation scale by
184 injecting particles to greater depth before decomposition begins^{51,52}, as determined by gut
185 retention time of migrating animals⁵¹⁻⁵³ and the depth of their migration (typically ~400 m⁵³).
186 The injected particles are zooplankton faecal pellets with sinking rates of 10-100’s m d⁻¹ (ref.
187 51), faster than loosely-packed organic aggregates settling from the surface^{11,12}, and will
188 penetrate deeper in the water column before remineralisation. This pump therefore influences
189 all important facets of the particle flux that govern carbon sequestration – total export rate,
190 depth of peak flux, and flux attenuation depth scale.

191 Diurnal vertical migration results in active subsurface transport and carbon sequestration, and
192 is usually reported for mesozooplankton and often included in BGP estimates⁵¹. However,
193 vertical migration by larger mesopelagic carnivorous organisms (from greater daytime depths
194 than mesozooplankton) are not sampled by conventional BGP approaches^{52,54}. Targeted
195 studies (Box 1) have quantified this pump driven by large mesopelagic migrant carnivores in
196 the Pacific⁵⁴, and other regions (S-Table 1). The underlying mechanism is upward migration
197 to graze mesozooplankton⁵⁴ followed by rapid (hours) downward migration⁵³, with
198 respiration (release of CO₂), exudation, and defecation (release of POC/DOC)^{51,55} often
199 below the permanent pycnocline⁵⁶, at depths up to 600m (Box 1).

200 Trawl surveys suggest that ~50% of mesopelagic organisms migrate, ranging regionally
201 between 20-90% depending on temperature, turbidity and oxygen concentrations^{54,56}. The
202 carbon sequestration rate by this pathway is governed by the metabolic transfer efficiency of
203 migrators, and particles are injected at their residence depth, often at the upper boundary of
204 oxygen minimum zones where their respiration intensifies oxygen depletion⁵³.

205 Active transport by vertically-migrating metazoans can also occur on longer timescales (Box
206 1). For example, in high latitude regions the winter hibernation of copepods (members of the
207 mesozooplankton) at depths between 600-1400m gives rise to a so-called ‘seasonal lipid
208 pump’³⁰: during hibernation, they catabolise carbon-rich lipids accumulated during summer in
209 upper layers and thereby shunt carbon (but not nitrogen and phosphorus) below the
210 permanent pycnocline³⁰. The strength of the seasonal lipid pump is governed by copepod
211 abundance, size and temperature, which together control their respiration rate and help
212 explain the existence of carbon flux hotspots (i.e. patchiness)³⁰.

213 Another vertical export mechanism that operates on seasonal migration timescales is
214 mortality at depth of hibernating zooplankton particularly in high latitude regions^{57,58},
215 sequestering carbon to depths >500 m depth. Global extrapolation of seasonal lipid pump
216 fluxes, along with the over-wintering mortality flux is problematic due to difficulties in
217 sampling and generalizing across distinct regional mechanisms³⁰ (S-Table 1).

218

219 **The potential for double accounting**

220 The export flux from the BGP is mediated by sinking particles, whereas PIPs can provide
221 additional pathways for all particle classes, from suspended to sinking, to exit the surface
222 ocean (Fig. 1). Thus, there is potential overlap between particles delivered from the surface
223 ocean to depth via the BGP and by injection from PIPs. Such overlap – termed here as

224 ‘double-accounting’ – may occur where particles associated with the BGP and a PIP are
225 difficult to distinguish and hence could be attributed to more than one pump (Fig. 1). At
226 depth, transformations such as aggregation alter particle characteristics, including size and
227 sinking rate, and hence particles injected by the PIPs can join the sinking flux usually
228 attributed the BGP (Fig. 1). A further factor that introduces overlap between the BGP and
229 PIPs results from the inclusion, for historical reasons⁵⁹, of one component of the mesopelagic
230 migration pump (diurnal migration by mesozooplankton) into the 1D sampling framework of
231 the BGP, while other components (e.g. patchier diurnal migration by larger mesopelagic
232 carnivores⁵) are not. Hence double-accounting can confound our understanding of the
233 relative importance of PIPs to ocean carbon storage.

234 Is it possible to tease apart these areas of overlap? Forty years study of the BGP has
235 uncovered a complex biogeochemical system with multiple drivers and distinguishing
236 characteristics^{11,60}. This body of research helps to frame the differences and similarities
237 between particles delivered to depth by PIP’s and those settling via the BGP. Each PIP is
238 distinct with respect to its combination of injected particle type (suspended cells to faecal
239 pellets of large mesopelagic migrants), the timing and depth of injection (Fig. 2a-b), and
240 associated particle transformations (aggregation/disaggregation)^{11,12,61}. Additionally, the
241 subsurface “fate” of particles (i.e. where they remineralize), which determines the longevity
242 of carbon sequestration, is driven by the complex interplay between these properties and
243 transformations^{12,60,61}: Particle composition and architecture set their sinking speed, while
244 myriad processes that are biologically- (microbes/zooplankton) and physically-mediated
245 (fragmentation/ disaggregation)^{12,62-64} decompose and repackage them over depth (Fig. 1).
246 Therefore, particle fate provides another avenue to distinguish the contributions of PIPs from
247 the BGP.

248 To date, evidence on the subsurface fate of injected particles has been largely indirect^{27,28,49}.
249 Surveys of eddy-subduction pumps suggest that injected particles may be remineralised at
250 depths <200 m, based on ammonium peaks⁴⁹, time-series of biogeochemical gradients²⁸, or
251 particle modelling studies²⁷. In the NE Atlantic, reported high rates of particle
252 remineralisation (glider-based biogeochemical gradients) must be reconciled with concurrent
253 evidence of coincident, coherent chlorophyll plumes at depths >300 m indicative of
254 subducted viable phytoplankton²⁸. This glider-based time-series reveals pronounced
255 patchiness²⁸ suggesting that inference of the fate of injected particles even from state-of-the-
256 art observations is challenging.

257 Better constraining the contribution of each PIP to mesopelagic carbon budgets will require
258 characterisation of the injected particle assemblage and their transformations during
259 downwards transport^{12,65-68}. Particle aggregation in PIPs may be driven by
260 convergence/subduction⁶⁹⁻⁷⁰ and/or differential sinking^{65,67}, potentially leading to altered
261 modes of subsurface transport (Fig. 1). BGC-Argo profile observations allow quantification
262 of the size, type, seasonal succession, and penetration depths of particles injected by the
263 mixed-layer pump³⁶ – properties which have the potential to differentiate them from fast-
264 sinking particles (i.e., BGP) whose distinctive ‘spiky’ bio-optical signature is readily detected
265 using multiple sensors⁷¹ (S-Figs. 2 and 3). Advances in bio-optics are already making cryptic
266 signatures associated with slow-sinking particles and zooplankton vertical migration less
267 opaque, lessening the possibility of double-accounting. Such double-accounting may be
268 avoided through the identification of unique characteristics of pumps including seasonality
269 (Fig. 2a), distinctive regional features³⁰, or multi-variate oceanographic diagnostics⁷².

270

271

272 **Carbon sequestration potential**

273 The potential carbon sequestration by each PIP can be quantified as the product of their
274 carbon injection rate and their sequestration timescale, i.e. time until remineralised carbon is
275 returned to the surface (see Supplementary Methods). This timescale is determined both by
276 the injection depth of particles and their eventual fate, i.e. the degree to which they sink or
277 circulate through the ocean before remineralising to CO₂. In general, deeper particle injection
278 and rapid sinking translates to longer carbon sequestration because the “passage time” from
279 the ocean interior to the surface increases with depth (Fig. 2b). Here, we assemble prior
280 estimates of carbon injection rate and depth (S-Table 1), along with new modelling
281 projections (Fig. 2), to estimate carbon sequestration by each PIP and assess their
282 significance relative to the BGP.

283 Some targeted studies provide concurrent estimates of carbon injection by individual PIPs
284 and the BGP^{27,28}, whereas others^{30,54,57,58} facilitate comparison of regional-scale PIP fluxes
285 with independent estimates of the BGP. Both approaches reveal that PIPs each have the
286 potential to contribute significant rates of POC export. The reported upper bounds of global
287 PIP estimates summed together is 8.7 Pg C yr⁻¹, which is comparable to the BGP export flux
288 (Table S1). This comprises 1.1-2.1 Pg C yr⁻¹ for the large-scale/mesoscale physical pumps
289 (also includes DOC^{22,23}), and 0.25-1.0, 0.9-3.6 and (-0.09) to 2.0 Pg C yr⁻¹ from the lipid
290 seasonal, mesopelagic migration, and eddy-subduction pumps, respectively (Fig. 2c). Thus,
291 their cumulative contribution may be as much as ~40% of total particle export (i.e.,
292 BGP+PIPs) suggesting considerable potential to resolve the imbalances reported for
293 mesopelagic carbon demand¹⁷, between nutrient and carbon export budgets¹⁵, and to lessen
294 the variability between model estimates of global carbon sequestration (S-Table 1).

295 We estimated the sequestration timescales for each PIP based on the “passage time” from the
296 injection depth to the surface in an observationally-constrained ocean circulation model¹⁴.
297 Particles injected at the depth of the wintertime mixed-layer by the large-scale physical
298 pumps (mixed-layer and subduction) result in sequestration for 25-100 years, assuming
299 subduction occurs before re-entrainment next winter. In turn, deeper injection by the eddy
300 subduction pump (up to 450 m), mesopelagic migration pump (up to 600 m), and seasonal
301 lipid pump (up to 1400 m) translates to sequestration timescales up to 150, 250, and 500
302 years respectively (Fig. 2b). These timescales will increase if it is assumed that sinking rather
303 than suspended particles are injected, which remineralise deeper than the injection horizon
304 (see Supplementary Methods).

305 Given the wide-ranging estimates of carbon injection rate (Fig. 2c) and depth (Fig. 2b) for
306 each PIP, oceanic carbon sequestration by these mechanisms cannot be estimated with
307 precision (Fig. 2d). However, choosing central values from the reported ranges of each
308 property allows a first order comparison between PIPs and the BGP. The mesopelagic
309 migration pump emerges as the most significant PIP, potentially storing ~60% as much
310 carbon as the BGP in the ocean interior if large, sinking particles (i.e. faecal pellets) are
311 injected. The C storage potential of the seasonal lipid, eddy-subduction and large subduction
312 pumps are ~20%, 10% and 5% of the BGP respectively, assuming each injects suspended
313 particles. The latter small net value is due to offsetting of subduction by strong obduction
314 (upward transport of water parcels) in the equatorial oceans³⁹. Based on these central values
315 (Fig. 2d), it is likely that the reservoir of respired carbon in the ocean interior contributed by
316 the PIPs approaches that contributed by the BGP, and may therefore help to close global-
317 scale mesopelagic carbon budgets^{15,16}.

318

319 **Tracer constraints on the fate of exported carbon**

320 Oceanic carbon sequestration by the BGP and wide-ranging biophysical mechanisms that
321 inject biogenic particles to depth depends critically on the fate of exported carbon (Fig. 2).
322 However, at present tracing the remineralisation of particles (regardless of their export
323 pathway) as they settle and circulate through the global ocean remains a logistical challenge,
324 due to the difficulties of deep-water particle sampling. Recently, new methods have used 3D
325 ocean data assimilation models to leverage geochemical “remineralisation tracers” including
326 oxygen and nutrients. These tracers integrate particle remineralisation signatures over long
327 timescales, and their global distributions are characterised by orders of magnitude more
328 observations than are available for particles^{16,31,73}. Two distinct approaches have been applied.
329 The first diagnoses remineralisation rates directly from phosphate accumulation along
330 transport pathways in a circulation model, and reconstructs particulate flux profiles required
331 to explain the global distribution of remineralised phosphate³¹. The second assimilates
332 geochemical and satellite data into mechanistic biogeochemical models to optimise key
333 particle flux parameters, yielding mechanistic insights while leveraging the observations less
334 directly⁷³.

335 Both approaches have yielded similar results and provide evidence for regional variability in
336 particle flux attenuation, with the flux attenuating slowly at high latitudes and quickly in
337 subtropical gyres, while the tropics lie between these two extremes (Fig. 3a). These
338 simulations reveal that carbon exported from high latitude and tropical surface waters is
339 sequestered longer in the oceans’ interior than carbon exported in the oligotrophic gyres
340 (Figure 3b), with important implications for feedbacks between the particle export and global
341 climate. Atmospheric pCO₂ is likely more sensitive to past changes in high latitude export
342 than previously recognised⁸, and the future expansion of subtropical habitats⁹ may result in
343 less efficient (although not currently quantifiable) carbon sequestration in a warming world.

344 Regional variations in particle flux attenuation have largely been interpreted in terms of the
345 balance between decomposition and sinking rates³². A likely explanation for the diagnosed
346 latitudinal pattern is the temperature-dependent metabolism of heterotrophs responsible for
347 particle decomposition^{32,73}, although variations in particle size and/or ballast are valid
348 alternatives⁷³. There may also be a secondary effect of oxygen, with decomposition slowing
349 in anoxic zones^{73,74}, and even hypoxic waters due to anaerobic microenvironment formation
350 in particles⁷⁵.

351 To some degree, model-derived particle flux profiles may also reflect the relative magnitude
352 of different export pathways (PIPs and BGP), which vary in the injection depth and nature of
353 particles they supply, since geochemical tracers integrate the effects of all export mechanisms.
354 Deep injection by PIPs would result in slower flux attenuation over depth, whereas injection
355 of suspended particles that remineralise shallower in the water column would be diagnosed as
356 rapid flux attenuation. Predicting future changes in ocean carbon sequestration will require a
357 better understanding of the contribution of injection versus remineralisation processes to
358 sequestration efficiency (Fig. 3b), given the different environmental sensitivity of these
359 processes.

360 The need for prediction motivates development of new techniques to distinguish particle flux
361 associated with the BGP and each PIP. Particle stoichiometry (i.e., C:N:P) may be central to
362 identifying particular mechanisms that decouple their export. For example, diagnosing
363 oxygen consumption between 500-1500 m (depth of zooplankton hibernation) without
364 concomitant nutrient accumulation would point to carbon export by the seasonal lipid pump³⁰.
365 Alternatively, diagnosing seasonal cycles of nutrient accumulation and oxygen consumption
366 rates would help distinguish remineralisation of particles exported by physical pumps versus
367 particle settling, which should exhibit distinct seasonality (Fig. 2a). This approach may soon

368 be possible given the burgeoning spatial/temporal resolution of tracer data provided by BGC-
369 Argo floats (S-Figure 1), and emerging float sensor technology (S-Table 2).

370

371 **Extrapolation – towards a 4D view of particle export**

372 Improving the accuracy of the initial estimates of the magnitude of carbon sequestration
373 presented in Figure 2d requires the development of a 4D picture of particle flux and storage
374 in the oceans' interior. It is clear from our synthesis of PIP mechanisms that multiple scales,
375 from sub-mesoscale to basin, must be accommodated if PIPs are to be assembled, first
376 spatially and then temporally, into a complete 4D picture. Again, lessons on how to approach
377 such upscaling can be gleaned from BGP research which imprinted both spatial and seasonal
378 signatures (satellite remote-sensing/modelling)²⁶ onto short-term (days-weeks) observations
379 taken at specific sites (Box 1). The timescales and lifetimes of features such as submesoscale
380 eddies/fronts or seasonal mesopelagic export signatures (Fig. 2a) must be characterized to
381 define the temporal footprint of each PIP and move towards a 4D viewpoint. This framework
382 must be linked to the seasonality of pelagic particle production to assess if there is distinctive
383 period for the subduction of significant stocks of these upper ocean particles (Fig. 2a). For
384 example, it is well-established that submesoscale dynamics are strongly seasonal, with
385 stronger and deeper penetration during winter than summer⁷⁶.

386 Some published approaches towards extrapolating PIP's globally, and to climatological time
387 scales, are outlined in S-Table 1. The identification of the specific drivers of each PIP
388 mechanism should help improve modelling and hence extrapolation. We advocate the utility
389 of explicitly incorporating the different PIP mechanisms into predictive, mechanistic models
390 as a means to extrapolate PIPs into 4D. In the case of the extrapolation of the submesoscale
391 eddy subduction PIP, increasing the model grid resolution to incorporate these features is

392 necessary and is now achievable in regional configurations^{77,78}. In contrast, other physically-
393 mediated PIPs such as the large-scale subduction and mixed-layer pumps are already
394 represented in global models, and so their extrapolation requires the development of
395 diagnostics to enable the simulated POC/DOC distributions to be better evaluated against
396 observations²³. At present, the biologically-mediated PIPs are not incorporated into state-of-
397 the-art biogeochemical models^{9,14,31,77,78}. While simulating animal behaviour at the global
398 scale remains a grand challenge in ocean modelling, simple parameterisations have been
399 developed to predict the geochemical effect of the mesopelagic migrant pump⁶, which might
400 be further expanded to incorporate hibernation and therefore the seasonal lipid pump. It is
401 only very recently that diel vertical migration has been incorporated for the first time in a
402 global ocean general circulation model and used to estimate the associated flux of carbon at
403 the global scale (see Aumont et al. in S-Table 1). Although promising, this approach remains
404 challenging because it is based on a computationally-intensive, end-to-end ecosystem model
405 in which all trophic levels from phytoplankton to top predators interact.

406

407 **Transforming our view of ocean carbon export**

408 Our synthesis of physically- and biologically-mediated PIPs reveals that they are directly
409 transporting significant stocks of biogenic particles to depth, of a cumulative magnitude that
410 may be equivalent to the carbon storage of the BGP. The potential of PIPs to make a major
411 contribution to the ocean carbon budget must now be explored in more detail, commencing
412 with those PIPs that are most likely to contribute to carbon sequestration. Synthesising
413 estimates of particle export, injection depth, and circulation timescales reveals that the
414 mesopelagic migrant pump has the greatest potential to contribute to carbon sequestration,
415 followed by the seasonal lipid pump and the various physical pumps (Fig. 2d). In the case of

416 the seasonal lipid pump, its geographical realm of influence is already established³⁰, whereas
417 less is known about the regional contributions of the mesopelagic migrant pump⁵.

418 For all PIPs, the most pressing research issue – needed to address double-accounting issues
419 and improve estimates of carbon sequestration – is to better understand the mechanisms of
420 particle transformations^{17,65-68} (Fig. 1) within a 4D framework. Specifically, the fate of
421 exported particles between their injection depth and the permanent pycnocline remains poorly
422 constrained. A first step will be improved particle characterisation, in particular the ability to
423 distinguish zooplankton from other particle types, and to aggregate Particle Size Distribution
424 (PSD) profiles through the development and application of new sensors (S-Table 2). Future
425 development of acoustic and imaging technologies⁷⁹ must be deployed on a range of
426 platforms from ships (i.e., calibration) to an array of long-lived (i.e., years), geographically-
427 diverse BGC-Argo floats. These developments towards improving particle characterisation
428 will reduce the likelihood of double-accounting. Moreover, the alignment of BGC-Argo
429 deployments (Box 1) with the characteristic space and time scales of PIPs will enable better
430 quantification of the role of patchiness in driving observed local/regional hotspots in
431 biological PIPs^{30,54,56}. In time, following the development and testing of a Coastal-Argo
432 platform, they can also be deployed to coastal and shelf seas to explore the role of PIPs in
433 these regions (S-Table 2).

434 The way forward in refining estimates of the contribution of PIPs in closing the ocean carbon
435 budget¹⁵⁻¹⁷ also requires leveraging advancements in ocean biogeochemical modelling.

436 Models are valuable testbeds to probe the sensitivity of carbon storage mechanisms, and
437 guide future observations. For example, model sensitivity analyses point to the pivotal role
438 of PSD in determining the fate of exported carbon^{31,73}, but the processes that set the PSD of
439 exported particles and its evolution over depth remain crudely parameterized. Developing
440 robust models of particle transformations between multiple size classes, and incorporating

441 them into general circulation models, will allow us to trace the fate of particles injected by
442 different PIPS and dissect their contribution to carbon sequestration, while avoiding double-
443 accounting issues.

444 Inverse methods that can assimilate PSD fields from new BGC-Argo technologies⁸⁰ will
445 allow models to “learn” from the data, further refining them to best reflect the real ocean.

446 Furthermore, downscaling of physical models is essential to simulate the locations of PIP
447 injections in support of observational programmes such as high resolution altimetry⁸¹, and the
448 integration of detailed particle transformations into submesoscale models⁸².

449 To transform the comprehension of particle export from one- to three- and eventually four-
450 dimensions, machine learning approaches⁸³ will need to be employed, which can be trained to
451 predict unknown variables such as particle flux from better sampled variables. Approaches
452 like artificial neural networks⁸⁴, will enable and enhance the upscaling of local/regional
453 datasets needed to provide more robust extrapolation^{85,86} to depth, regionally, and annually of
454 each PIP. This upscaling is essential to refine estimates of the contribution of each PIP to
455 carbon sequestration. BGC-Argo datasets will also eventually be combined with new satellite
456 products such as hyperspectrally-resolved ocean colour observations of biology processes⁸⁷
457 and submesoscale characterisation of sea level using high-resolution altimetry⁸¹.

458 Satellite and water-column remote-sensing, along with targeted process studies, will yield
459 expansive datasets that can be assimilated into regional and global models of ever increasing
460 realism and resolution. Together, these approaches will lead towards a robust, four-
461 dimensional view of carbon sequestration by the ocean’s multi-faceted bio-physical particle
462 pumps.

463

464

465 Acknowledgements

466 The authors thank five anonymous reviewers for improving the manuscript. PWB was
467 primarily supported by the Australian Research Council through a Laureate (FL160100131),
468 and this research was also supported under Australian Research Council's Special Research
469 Initiative for Antarctic Gateway Partnership (Project ID SR140300001). HC acknowledges
470 the support of the European Research Council (remOcean project, grant agreement 246777)
471 and of the Climate Initiative of the BNP Paribas foundation (SOCLIM project). ML was
472 supported by CNES and by the ANR project SOBUMS (ANR-16-CE01-0014). DAS
473 acknowledges support from the National Aeronautics and Space Administration as part of the
474 EXport Processes in the global Ocean from RemoTe Sensing (EXPORTS) field campaign -
475 grant 80NSSC17K0692. TW was supported by NSF grant OCE-1635414. Co-authors, HC,
476 ML, DS and TW contributed equally to this Review.

477

478

479

480

481

482

483

484

485

486

487

488

489

490

491

492

493

494

495

496

497

498

499 References

- 500 1Sarmiento, J. L. & Gruber, N. (2006). *Ocean Biogeochemical Dynamics*. (Princeton
501 University Press, 2006).
- 502 2Volk, T., and M. Hoffert (1985). Ocean carbon pumps: Analysis of relative strengths and
503 efficiencies in ocean-driven atmospheric CO₂ changes, in *The Carbon Cycle and*
504 *Atmospheric CO₂: Natural Variations Archean to Present*, Geophys. Monogr. Ser., vol. 32,
505 edited by E. T. Sundquist and W. S. Broecker, pp. 99–110, AGU, Washington, D. C.
- 506 3McKinley GA, Pilcher DJ, Fay AR, Lindsay K, Long MC, Lovenduski NS. (2016).
507 Timescales for detection of trends in the ocean carbon sink. *Nature* 530:469–72
- 508 4Buesseler, K. O., Lamborg, C. H., Boyd, P. W., Lam, P. J., Trull, T. W., and co-authors
509 (2007). Revisiting carbon flux through the ocean's twilight zone through the ocean's twilight
510 zone. *Science*, 316, 567-570. doi: 10.1126/science.1137959.
- 511 5Irigoiien, X. et al. (2014). Large mesopelagic fishes biomass and trophic efficiency in the
512 open ocean. *Nat. Commun.* 5, ncomms4271.
- 513 6Maier-Reimer E., U. Mikolajewicz, A. Winguth (1996). Future ocean uptake of CO₂:
514 interaction between ocean circulation and biology. *Climate Dynamics*, 12, 711-721.
- 515 7Bopp, L., et al. (2013), Multiple stressors of ocean ecosystems in the 21st century:
516 Projections with CMIP5 models, *Biogeosciences*, 10, 6225–6245.
- 517 8Martinez-Garcia, A. et al. (2014). Iron fertilization of the Subantarctic Ocean during the last
518 ice age. *Science* 343, 1347–1350.
- 519 9Moore J.K. et al. (2018) Sustained climate warming drives declining marine biological
520 productivity. *Science*, 2018; 359 (6380): 1139 DOI: 10.1126/science.aao6379
- 521 10Bernardello R. et al. (2015) Response of the ocean natural carbon storage to projected
522 twenty-first-century climate change *J of Climate* DOI: 10.1175/JCLI-D-13-00343.1
- 523 11Boyd, P. W. & Trull, T. W. (2007). Understanding the export of biogenic particles in
524 oceanic waters: Is there consensus? *Progress in Oceanography*, 72(4), 276-312. doi:
525 10.1016/j.pocean.2006.10.007
- 526 12Buesseler, K.O., and Boyd, P.W. (2009). Shedding light on processes that control particle
527 export and flux attenuation in the twilight zone of the open ocean. *Limnol. Oceanogr.* 54,
528 1210–1232.doi:10.4319/lo.2009.54.4.1210
- 529 13Martin, J., G. Knauer, D. Karl, and W. Broenkow (1987), VERTEX: Carbon cycling in the
530 northeast Pacific, *Deep Sea Res., Part A*, 34, 267–285.
- 531 14DeVries, T., F. Primeau, and C. Deutsch (2012). The sequestration efficiency of the
532 biological pump, *Geophysical Research Letters*, 39, doi:10.1029/2012GL051963.
- 533 15Emerson, S. (2014) Annual net community production and the biological carbon flux in the
534 ocean. *Global Biogeochemical Cycles* 28, 1–12, doi:10.1002/2013GB004680

- 535 16Schlitzer, R. (2002) Carbon export fluxes in the Southern Ocean: results from inverse
536 modeling and comparison with satellite based estimates, *Deep-Sea Research II*, 49, 1623-
537 1644.
- 538 17Burd, A. B. et al. (2010). Assessing the apparent imbalance between geochemical and
539 biochemical indicators of meso- and bathypelagic biological activity: What the @#! is
540 wrong with present calculations of carbon budgets? *Deep-Sea Res. Part II Top. Stud.*
541 *Oceanogr.* 57: 1557–1571. doi:10.1016/j.dsr2.2010.02.022
- 542 **This paper reviewed the (lack of) progress on constraining mesopelagic carbon budgets,**
543 **and advocated new approaches to tackle this issue.**
- 544 18Giering, S. L. et al. (2014). Reconciliation of the carbon budget in the ocean’s twilight
545 zone. *Nature* 507, 480–483. doi: 10.1038/nature13123
- 546 **This paper presented one of the few balanced mesopelagic carbon budgets by assessing**
547 **community respiration versus carbon demand.**
- 548 19Steinberg, D.K., B.A.S. Van Mooy, K.O. Buesseler, P. W. Boyd, T. Kobari, and D.M. Karl
549 (2008). Bacterial vs. zooplankton control of sinking particle flux in the ocean’s twilight zone.
550 *Limnol. Oceanogr.* 53: 1327–1338.
- 551 20Reinthal, T. et al. (2006). Prokaryotic respiration and production in the meso- and
552 bathypelagic realm of the eastern and western North Atlantic basin. *Limnol. Oceanogr.* 51:
553 1262–1273.
- 554 21Boyd, P.W., McDonnell, A., Valdez, J. (2015) RESPIRE: An in situ particle interceptor to
555 conduct particle remineralization and microbial dynamics studies in the oceans' Twilight
556 Zone. *Limnology and Oceanography-Methods* Volume: 13s: 494-508.
- 557 22Hansell D.A., Carlson C.A., Repeta D.J., Schlitzer R., (2009). Dissolved organic matter in
558 the ocean. *Oceanography* 22:52–61.
- 559 23Lévy, M., Bopp, L., Karleskind, P., Resplandy, L., Ethé, C., & Pinsard, F. (2013). Physical
560 pathways for carbon transfers between the surface mixed layer and the ocean interior. *Global*
561 *Biogeochemical Cycles*, 27(4), 1001–1012. <http://doi.org/10.1002/gbc.20092>.
- 562 24Henson, S. A., Yool, A., & Sanders, R. (2015). Variability in efficiency of particulate
563 organic carbon export: A model study. *Geophysical Res. Lett.*, 29, 33–45.
564 <http://doi.org/doi:10.1002/2014GB004965>
- 565 25Aumont, O., Van Hulst, M., Roy-Barman, M., Dutay, J.-C., Ethé, C., & Gehlen, M.
566 (2017). Variable reactivity of particulate organic matter in a global ocean biogeochemical
567 model. *Biogeosciences*, 14(9), 2321–2341. <http://doi.org/10.5194/bg-14-2321-201713>
- 568 26Siegel, D. A., K. O. Buesseler, S. C. Doney, S. F. Sailley, M. J. Behrenfeld, and P. W.
569 Boyd (2014), Global assessment of ocean carbon export by combining satellite observations
570 and food-web models, *Global Biogeochem. Cycles*, 28, 181–196,
571 doi:10.1002/2013GB004743.
- 572 27Stukel M.R., H. Song, R. Goericke, A.J. Miller (2017) The role of subduction and
573 gravitational sinking in particle export, carbon sequestration, and the remineralization length

574 scale in the California Current Ecosystem. *Limnology and Oceanography*, doi:
575 10.1002/lno.10636

576 28Omand, M.M. et al. (2015). Eddy-driven subduction exports particulate organic carbon
577 from the spring bloom. *Science* 348,222–225.doi:10.1126/science.1260062.

578 **This paper quantified the Eddy Subduction Pump (ESP) using an array of gliders in the**
579 **North Atlantic during the spring bloom.**

580 29Dall’Olmo G., J. Dingle, L. Polimene, R.J.W. Brewin and H.Claustre (2016). Substantial
581 energy input to the mesopelagic ecosystem from the seasonal mixed-layer pump. *Nature*
582 *Geoscience*, 9, 820-825 DOI: 10.1038/NGEO2818.

583 **This paper quantified the Mixed Layer Pump (MLP) across large regions of the high**
584 **latitude ocean.**

585 30 Jónasdóttir S.H, Richardson K., Heath M.R. 2015. Seasonal copepod lipid pump promotes
586 carbon sequestration in the deep North Atlantic. *PNAS* 112:12122–26.

587 **This paper provided the first detailed quantification of the seasonal lipid pump (SLP).**

588 31Weber T. et al. (2016), Deep ocean nutrients imply large latitudinal variation in particle
589 transfer efficiency. *PNAS*, 113, 8606–8611.

590 32Marsay, C. M., R. J. Sanders, S. A. Henson, K. Pabortsava, E. P. Achterberg, and R. S.
591 Lampitt (2015), Attenuation of sinking particulate organic carbon flux through the
592 mesopelagic ocean, *Proc. Natl. Acad. Sci. U.S.A*, 112, 1089–1094.

593 32Giering, S. L. C., R. Sanders, A. P. Martin, S. A. Henson, J. S. Riley, C. M. Marsay, and D.
594 G. Johns (2017), Particle flux in the oceans: Challenging the steady state assumption, *Global*
595 *Biogeochem. Cycles*, 31, 159–171, doi: 10.1002/2016GB005424.

596 34Jiao N., et al. 2010. Microbial production of recalcitrant dissolved organic matter: long-
597 term carbon storage in the global ocean. *Nat. Rev. Microbiol.* 8:593–599.

598 35Swan, B.K. et al. (2011) Potential for Chemolithoautotrophy Among Ubiquitous Bacteria
599 Lineages in the Dark Ocean. *Science*, 333, 1296-1300.

600 36Bishop, J. K. B., M. H. Conte, P. H. Wiebe, M. R. Roman, and C. Langdon (1986),
601 Particulate matter production and consumption in deep mixed layers: Observations in a
602 warm-core ring, *Deep Sea Res. Part A*, 33, 1813–1841.

603 37Dall’Olmo, G., and K. A. Mork (2014), Carbon export by small particles in the Norwegian
604 Sea, *Geophys. Res. Lett.*, 41, 2921–2927, doi:10.1002/2014GL059244.

605 38Cushman-Roisin, B. (1987). Subduction. Hawaii Univ, Dynamics of the Oceanic Surface
606 Mixed Layer P 181-196.

607 39Marshall, J., Nurser, A. & Williams, R. Inferring the subduction rate and period over the
608 North Atlantic. *J. Phys. Oceanogr.* 23, 1315–1329 (1993).

609 40Liu, L. L., Huang, R. X., 2012. (2012). The global subduction/obduction rates: Their
610 interannual and decadal variability. *Journal of Climate*, 25(4), 1096–1115.
611 <http://doi.org/10.1175/2011JCLI4228.1>

612
613 41Pollard R. T. & L. Regier (1990) Large variations in potential vorticity at small spatial
614 scales in the upper ocean. *Nature* 348, 227–229 doi:10.1038/348227a0.

615 42Nurser, A., & Zhang, J. (2000). Eddy-induced mixed layer shallowing and mixed
616 layer/thermocline exchange. *Journal of Geophysical Research Ocean*, 105(C9), 21851.

617 43Niewiadomska, K., Claustre, H., Prieur, L., & D’Ortenzio, F. (2008). Submesoscale
618 physical-biogeochemical coupling across the Ligurian Current (northwestern Mediterranean)
619 using a bio-optical glider. *Limnol. Oceanogr*, 53, 2210–2225.

620 44Estapa, M. L., D. A. Siegel, K. O. Buesseler, R. H. R. Stanley, M. W. Lomas, and N. B.
621 Nelson (2015), Decoupling of net community and export production on submesoscales in the
622 Sargasso Sea, *Global Biogeochem. Cycles*, 29, 1266–1282, doi:10.1002/2014GB004913

623 45Lévy, M, Klein, P. and A.-M. Treguer (2001). Impacts of sub-mesoscale physics on
624 phytoplankton production and subduction, *J. Mar. Res.*, 59,535-565 doi:
625 10.1357/002224001762842181

626 46Nagai, T., Gruber, N., Frenzel, H., Lachkar, Z., McWilliams, J. C., & Plattner, G.-K.
627 (2015). Dominant role of eddies and filaments in the offshore transport of carbon and
628 nutrients in the California Current System. *J. Geophys. Res. Ocean*,
629 <http://doi.org/10.1002/2015JC010889>

630 47Karleskind, P., Lévy, M., & Memery, L. (2011). Modifications of mode water properties
631 by sub-mesoscales in a bio-physical model of the Northeast Atlantic. *Ocean Modelling*, 39,
632 47–60.

633 48Karleskind, P., Lévy, M., & Memery, L. (2011). Subduction of carbon, nitrogen, and
634 oxygen in the northeast Atlantic. *Journal of Geophysical Research Ocean*, 116(C2), C02025.
635 <http://doi.org/10.1029/2010JC006446>

636 49Stukel, M. R. et al. (2017). Mesoscale ocean fronts enhance carbon export due to
637 gravitational sinking and subduction. *Proc. Natl. Acad. Sci. USA*. 114: 1252–1257.
638 doi:10.1073/pnas.1609435114

639 **This paper compared the magnitude of export fluxes from the biological pump and the**
640 **Eddy Subduction Pump (ESP).**

641 50Vinogradov M.E. (1997) Some Problems of Vertical Distribution of Meso- and
642 Macroplankton in the Ocean. *Advances in Marine Biology* Volume 32, 1997, Pages 1-92.
643 [https://doi.org/10.1016/S0065-2881\(08\)60015-2](https://doi.org/10.1016/S0065-2881(08)60015-2)

644 51Steinberg D.K., and M.R. Landry (2017). Zooplankton and the ocean carbon cycle. *Annu.*
645 *Rev. Mar. Sci.* 2017. 9:413–44

646 52Bianchi D., Stock C., Galbraith E.D., Sarmiento J.L. (2013). Diel vertical migration:
647 ecological controls and impacts on the biological pump in a one-dimensional ocean model.
648 *Glob. Biogeochem. Cycles* 27:487–91

649 53Bianchi, D., Galbraith, E. D., Carozza, D. A., Mislan, K. A. S., & Stock, C. A. (2013).
650 Intensification of open-ocean oxygen depletion by vertically migrating animals. *Nature*
651 *Geoscience*, 6(7), 545.

652 **This paper used global Acoustic Doppler Current Profiler observations to constrain the**
653 **Mesopelagic Migration Pump.**

654 54Davison, P.C., Checkley Jr., D.M., Koslow, J.A., Barlow, J., (2013). Carbon export
655 mediated by mesopelagic fishes in the northeast Pacific Ocean. *Progress in Oceanography*
656 116, 14–30.

657 **This paper used trawl surveys and metabolic modelling to assess the export fluxes**
658 **mediated by mesopelagic fishes.**

659 55Childress, J. J., S. M. Taylor., G. M. Cailliet and M. H. Price (1980) Patterns of growth,
660 energy utilization and reproduction in some meso- and bathypelagic fishes off Southern
661 California. *Marine Biology* 61, 27-40 (1980)

662 56Klevjer T. A., X. Irigoien, A. Røstad, E. Fraile-Nuez, V. M. Benítez-Barrios & S.
663 Kaartvedt. (2016). Large scale patterns in vertical distribution and behaviour of mesopelagic
664 scattering layers. *Scientific Reports*, 6:19873, DOI: 10.1038/srep19873

665 57Bradford-Grieve JM, Nodder SD, Jillett JB, Currie K, Lassey KR. (2001). Potential
666 contribution that the copepod *Neocalanus tonsus* makes to downward carbon flux in the
667 Southern Ocean. *J. Plankton Res.* 23: 963– 75

668 58Kobari T, Steinberg DK, Ueda A, Tsuda A, Silver MW, Kitamura M. (2008). Impacts of
669 ontogenetically migrating copepods on downward carbon flux in the western subarctic Pacific
670 Ocean. *Deep-Sea Res. II*, 55:1648–60.

671 59Dam, H.G., C.A. Miller and S.H. Jonasdottir (1993) The trophic role of mesozooplankton
672 at 47N, 20W during the North Atlantic Bloom Experiment. *Deep-Sea Res. II*, 40, 197-212.

673 60Turner J.T. (2015). Zooplankton fecal pellets, marine snow, phytodetritus and the ocean's
674 biological pump. *Prog. Oceanogr.* 130:205–48

675 61Bishop, J.K.B. (1989) Regional extremes in particulate matter composition and flux:
676 effects on the chemistry of the ocean interior. W.H. Berger, V.S. Smetacek, G. Wefer (Eds.),
677 *Productivity of the ocean: present and past*, Dahlem Konferenzen, John Wiley & Sons, New
678 York (1989), pp. 117-137

679 62McDonnell, A. M. P., P. W. Boyd, K. O. Buesseler (2015) Effects of sinking velocities and
680 microbial respiration rates on the attenuation of particulate carbon fluxes through the
681 mesopelagic zone. *Global Biogeochemical Cycles*. DOI: 10.1002/2014GB004935.

682 63Durkin, C.A., M.L. Estapa, and K.O. Buesseler (2015) Observations of carbon export by
683 small sinking particles in the upper mesopelagic. *Marine Chemistry*, 175, 72-81.

684 64Cavan EL, Trimmer M, Shelley F, Sanders R, (2017) Remineralization of particulate
685 organic carbon in an ocean oxygen minimum zone, *Nature Communications*, 8 Article 14847.
686 ISSN 2041-1723.

687 65Aldredge, A.L., Silver, M.W., (1988). Characteristics, dynamics and significance of
688 marine snow. *Progress in Oceanography* 20, 41–82.

689 66Jackson, G.A. (1990) A model of the formation of marine algal flocs by physical
690 coagulation processes. *Deep Sea Research Part A. Oceanographic Research Papers* 37 (8),
691 1197-1211, 1990.

692 67Kjørboe, T., (2001). Formation and fate of marine snow: small-scale processes with large-
693 scale implications. *Scientia Marina* 65 (Suppl. 2), 57–71.

694 68Iversen, M.H., Ploug, H., (2013). Temperature effects on carbon-specific respiration rate
695 and sinking velocity of diatom aggregates – potential implications for deep ocean export
696 processes. *Biogeosciences* 10, 4073–4085.

697 69Ohman M.D., R. Powell, M. Picheral and D.W. Jensen (2010) Mesozooplankton and
698 particulate matter responses to a deep-water frontal system in the southern California Current
699 System *J. Plankton Res.* 34, 815–827.

700 70D'Asaro, E. A. et al. (2018). Ocean convergence and the dispersion of flotsam. *Proceedings*
701 *of the National Academy of Sciences*, 30, 201718453–6.
702 <http://doi.org/10.1073/pnas.1718453115>

703 71Briggs, N., M. J. Perry, I. Cetinic, C. Lee, E. D'Asaro, A. M. Gray, and E. Rehm (2011),
704 High-resolution observations of aggregate flux during a sub-polar North Atlantic spring
705 bloom, *Deep Sea Res. Part I*, 58(10), 1031–1039.

706 72Stanley R.H.R., D.J. McGillicuddy Jr. Z. O. Sandwith, H. M. Pleskow (2017)
707 Submesoscale hotspots of productivity and respiration: Insights from high resolution oxygen
708 and fluorescence sections. *Deep-Sea Research I*, <https://doi.org/10.1016/j.dsr.2017.10.005>

709 73DeVries, T., and T. Weber (2017), The export and fate of organic matter in the ocean: New
710 constraints from combining satellite and oceanographic tracer observations, *Global*
711 *Biogeochem. Cycles*, 31, 535–555, doi:10.1002/2016GB005551.

712 74Cram, J.A., T. Weber, S.W. Leung, A.M.P. McDonnell, J. H. Liang, C. Deutsch (2018),
713 The role of particle size, ballast, temperature, and oxygen in the sinking flux to the deep sea.
714 *Glob. Biogeo. Cyc.* <https://doi.org/10.1029/2017GB005710>.

715 75Bianchi D., T.S.Weber, R. Kiko, C. Deutsch (2018). Global niche of marine anaerobic
716 metabolisms expanded by particle microenvironments. *NGEO* in press.
717 <https://doi.org/10.1038/s41561-018-0081-0>.

718 76Callies, J., Ferrari, R., Klymak, J. M., & Gula, J. (2015). Seasonality in submesoscale
719 turbulence. *Nature Communications*, 6, 6862–9. <http://doi.org/10.1038/ncomms7862>

720 77 Lévy, M. et al. (2012). Large-scale impacts of submesoscale dynamics on phytoplankton:
721 Local and remote effects, 43-44(C), 77–93. <http://doi.org/10.1016/j.ocemod.2011.12.003>.

722 78Harrison, C. S., Long, M. C., Lovenduski, N. S., & Moore, J. K. (2018). Mesoscale effects
723 on carbon export: A global perspective. *Global Biogeochemical Cycles*, 32, 680–703.
724 <https://doi.org/10.1002/2017GB005751>

725 79Picheral, M., L. Guidi, L. Stemmann, D.M. Karl, G. Iddaoud Ghizlaine and G. Gorsky
726 (2010), The Underwater Vision Profiler 5: An advanced instrument for high spatial resolution

727 studies of particle size spectra and zooplankton, *Limnol. Oceanogr. Methods*, 8,
728 doi:10.4319/lom.2010.8.462.

729 80Johnson K. (2017). Biogeochemical sensors for autonomous, Lagrangian platforms:
730 Current status, future directions. *Autonomous and Lagrangian Platforms and Sensors ALPS*
731 II. <https://alps-ocean.us/agenda/>(last accessed 16 March 2017).

732 81Ubelmann, C. and L.-L. Fu, (2014) On the transition from profile altimeter to swath
733 altimeter for observing global ocean surface topography. *J. Atmos. Oceanic Tech.*, 31, 560-
734 568.

735 82Resplandy, L. et al. (2012). How does dynamical spatial variability impact ²³⁴Th-derived
736 estimates of organic export? *Deep Sea Res. I*, 68(C), 24–45.
737 <http://doi.org/10.1016/j.dsr.2012.05.015>

738 83Castelvecchi, D. (2016). Can we open the black box of AI? *Nature*, 528, 20-23.
739 doi:10.1038/538020a.

740 84Sauzède, R. et al. (2016). A neural network-based method for merging ocean color and
741 Argo data to extend surface bio-optical properties to depth: Retrieval of the particulate
742 backscattering coefficient. *Journal of Geophysical Research-Oceans*, 121(4), 2552-2571.
743 doi:10.1002/2015jc011408.

744 85Landschützer, P., N. Gruber, D. C. E. Bakker, U. Schuster, S. Nakaoka, M. R. Payne, T.
745 Sasse, and J. Zeng (2013), A neural network-based estimate of the seasonal to inter-annual
746 variability of the Atlantic Ocean carbon sink, *Biogeosciences*, 10, 7793–7815,
747 doi:10.5194/bg-10-7793-2013.

748 86Landschützer, P., N. Gruber, D.C.E. Bakker, and U. Schuster (2014). Recent variability of
749 the global ocean carbon sink. *Global Biogeochemical Cycles*, 28(9), 927-949.
750 doi:10.1002/2014gb004853.

751 87Werdell, P.J., L. I. W. McKinna, E. Boss, S. G. Ackleson, S. E. Craig, W. W. Gregg, Z.
752 Lee, S. Maritorea, C. S. Roesler, C. S. Rousseaux, D. Stramski, J. M. Sullivan, M. S.
753 Twardowski, M. Tzortziou, and X. Zhang, (2018), An overview of approaches and challenges
754 for retrieving marine inherent optical properties from ocean color remote sensing. *Prog.*
755 *Oceanogr.* 160, 186–212.

756 88Boyd, P.W. et al. (2005). The evolution and termination of an iron-induced mesoscale
757 bloom in the northeast subarctic Pacific Ocean. *Limnology and Oceanography* 50, 1872–
758 1886.

759 89Ohman, M.D., J.-B. Romagnan (2016) Nonlinear effects of body size and optical
760 attenuation on Diel Vertical Migration by zooplankton. *Limnol. Oceanogr.* 61, 2016, 765–
761 770.

762 90Powell, J.R., and M.D. Ohman (2012) Use of glider-class acoustic Doppler profilers for
763 estimating zooplankton biomass *J. Plankton. Res.*, 34, 563–568.

764 91Siegel, D. A., and W. G. Deuser. (1997). Trajectories of sinking particles in the Sargasso
765 Sea: Modeling of statistical funnels above deep-ocean sediment traps. *Deep-Sea Res. Part I*
766 *Oceanogr. Res. Pap.* 44: 1519–1541. doi:10.1016/S0967-0637(97)00028-9

767 92Siegel, D. A., E. Fields, and K. O. Buesseler (2008), A bottom-up view of the biological
768 pump: Modeling source funnels above ocean sediment traps, *Deep Sea Res. Part I*, 55(1),
769 108–127, doi:10.1016/j.dsr.2007.10.006.

770 93Llort, J., Langlais, C., Matear, R., Moreau, S., Lenton, A., Strutton, P.G., (2018).
771 Evaluating Southern Ocean carbon eddy-pump from biogeochemical Argo floats. *Journal of*
772 *Geophysical Research: Oceans*. <https://doi.org/10.1002/2017JC012861>

773

774

775

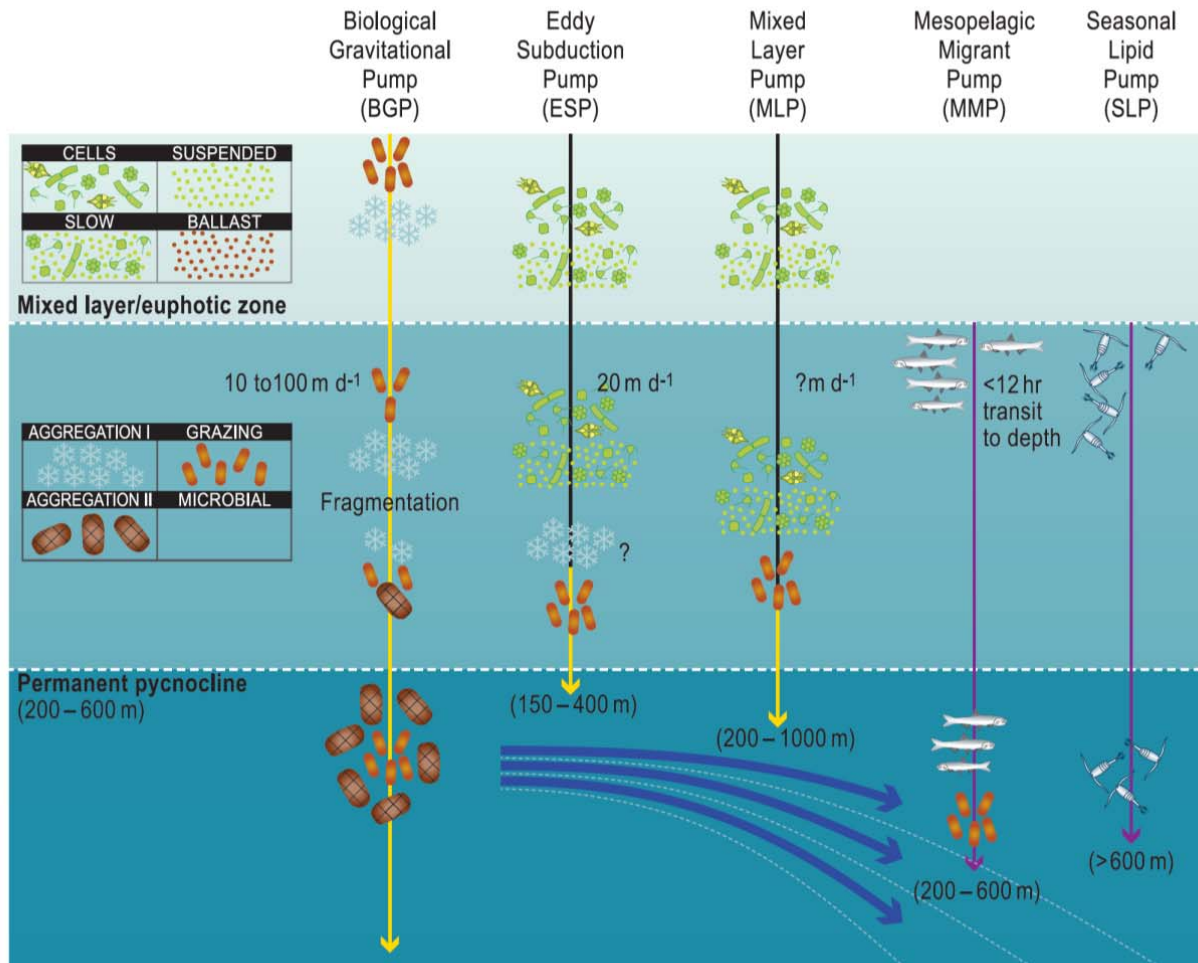


Figure 1 Interplay between particle characteristics, mode of export (BGP or PIP), delivery depth and larger scale ocean circulation for a range of pumps. In the upper panel, the box (top left) represents mixed-layer particle types, which either form large sinking particles (i.e., within the BGP, such as faecal pellets, marine snow) or are injected to depth (i.e., PIPs, suspended/ slow-settling heterogeneous particles and cells (i.e., including healthy, slow-sinking phytoplankton⁸⁸)). The vertical yellow arrow signifies the BGP; black lines physically mediated PIPs; and purple lines biologically mediated PIPs. The delivery rates of particles to subsurface strata (in m d⁻¹, ? denotes not known) are presented for each pump. Patchiness in the distribution of vertically-migrating animals (top right) plays a role in driving three-dimensional particle delivery to depth^{89,89}, and is denoted by different fish or copepod stocks in the upper ocean. The box (middle left) presents different particle transformations central to the BGP¹², but whose role is not known so far for PIPs. They include microbial solubilisation, aggregation (marine snow denoted by aggregation I; heterogeneous faecally-dominated aggregates (aggregation II) and/or disaggregation¹⁸ to form/break down heterogeneous particles (hatched brown symbols). In the lower panel, depths in parentheses are the reported delivery depths, with the BGP (and some PIPs) exporting some particles to the sea floor. Blue curved arrows represent transport of subsurface material along downward-sloping isopycnals (white dashed lines). Major unknowns include whether physical transport by PIPs can cause particle aggregation (signified by ? in the middle panel below subduction pump, and also applicable for the mixed-layer pump) and hence alter their mode of injection towards gravitational settling (i.e., the BGP). Other unknowns include the potential ballasting role of small mineral particles such as aerosol dust for PIPs.

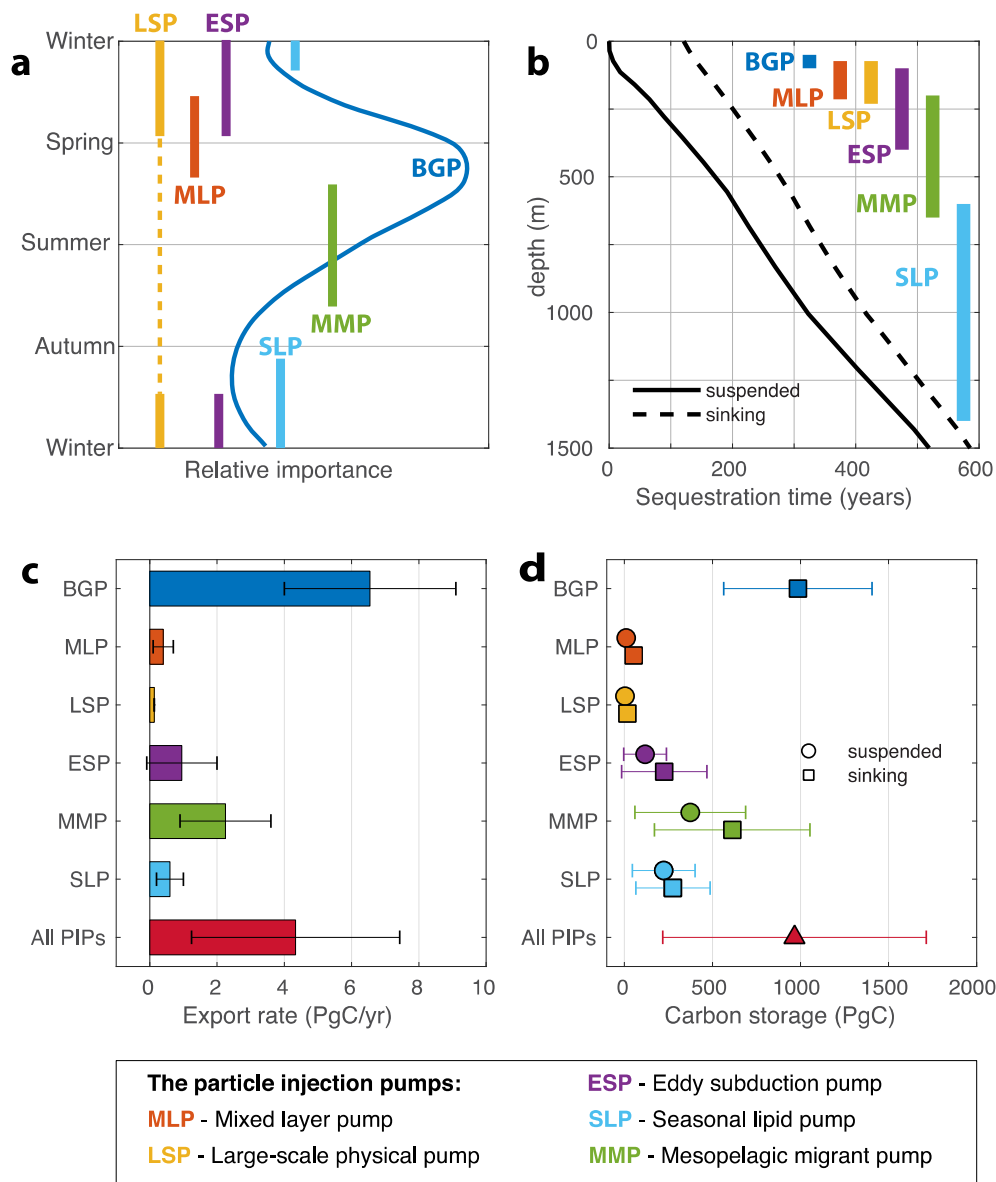


Figure 2 Carbon export and storage by PIPs compared to the BGP. **a)** Idealised seasonality of the PIPs for regions that exhibit strong seasonality, where a Spring Bloom dominates C export by the BGP (dark blue line). Coloured bars indicate season of peak C export by the PIPs (acronyms defined in legend). Note the large-scale physical pump should be strongest when mixed layers are deepest, but is likely operative all year (dashed line). **b)** Sequestration efficiency of the PIPs. Black lines represent the global-mean sequestration timescale for carbon injected at a given depth, defined as the time for remineralised carbon to circulate back to the ocean surface, computed in a data-constrained circulation model (see S-Methods). Solid line assumes that particles are suspended, so remineralisation occurs at the injection depth, whereas dashed line assumes that particles are sinking and remineralise over depth (see Methods). Colored bars show injection depth range of the BGP and PIPs. The efficiency of each pump is defined as the sequestration time from its injection depth. **c)** Strength of the pump mechanisms, defined as their rate of carbon export or injection (see Table S1). “All PIPs” refers to the sum of the five individual PIPs **d)** Ocean carbon storage by each pump, defined as the product of the strength (**c**) and efficiency (**b**). Two scenarios are shown for each PIP, using the sequestration time for suspended (circles) and sinking (square) particles, whereas the BGP is assumed to export only sinking particles. For the sum of PIPs, we present a “most likely” scenario, in which the migrant pump injects sinking particles (faecal pellets), and all other PIPs inject suspended particles (triangle).

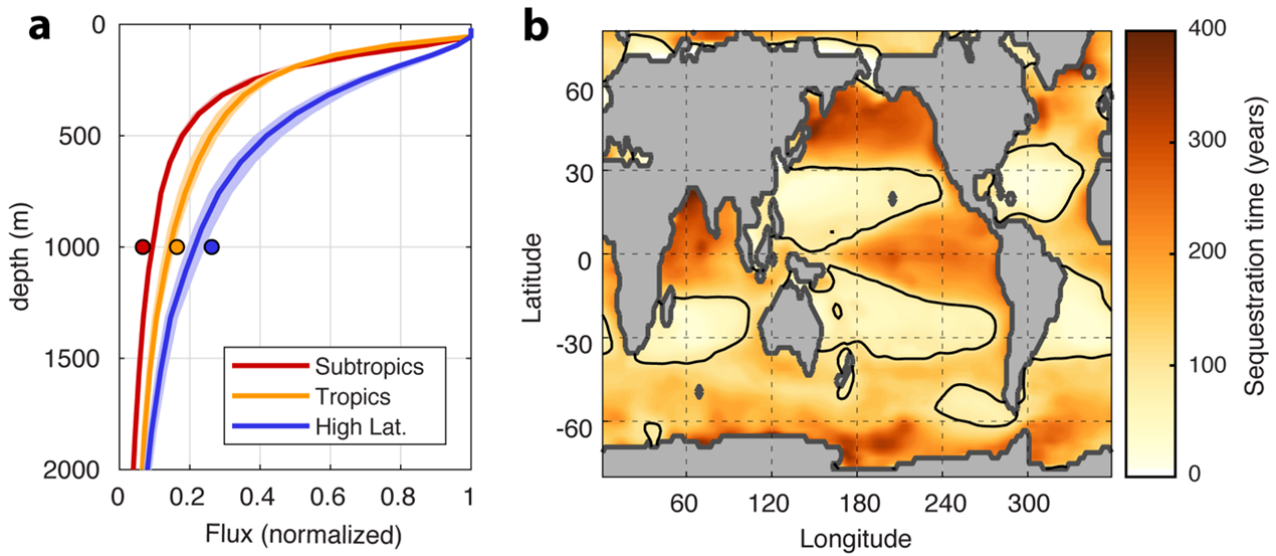


Figure 3. Fate of exported organic matter constrained in models from geochemical remineralisation tracers. a) Organic matter flux over depth (normalised to flux at the base of the euphotic zone), averaged across subtropics, tropics, and high latitude regions (as defined³¹). Lines show flux profiles from a mechanistic model⁷³ that is optimised to match geochemical constraints (shading represents the range between 12 model configurations); circles represent the transfer efficiency diagnosed directly from nutrient accumulation in an ocean circulation model³¹. **b)** Sequestration time of exported carbon. The spatial pattern reflects both variability in the particle flux attenuation (a), and patterns of large-scale circulation. The thin black lines separates regions of efficient (>100 years) and inefficient (<100 years) carbon sequestration.

Box 1 Approaches used to investigate downward particle export, from the BGP to PIPs.

The BGP is quantified in a biologically-patchy upper ocean (green filaments) using ship-based surface sampling (particle production) and subsurface particle interception by sediment traps, most recently neutrally-buoyant traps downstream of particle source regions (orange instruments, a). This coupled surface-subsurface sampling strategy is logistically-complex, temporally- and spatially-restricted (i.e., represented here by a “statistical funnel”^{91,92}, see a), and hence provides a ‘1D’ view of particle export that is extrapolated to the basin scale using satellite observations and/or modelling. This ‘1D’ viewpoint cannot measure the PIPs presented in b) to e), and is contrasted in a) with the 4D view^{29,93} obtained by an ensemble of BGC-Argo floats (white instruments).

(b) the mixed-layer pump, in which particles are detrained when the pycnocline (blue dashed line) shallows, can be addressed regionally through backscattering (a proxy for POC) profiles measured by BGC-Argo floats³⁶, or globally using satellite surface-ocean backscattering and Argo/BGC-Argo (density/backscattering) vertical profiles³². c) the seasonal lipid pump is quantified using surveys of overwintering copepods at depths below the permanent pycnocline and subsequent scaling of their lipid-enriched biomass in carbon content³³. d) the eddy subduction pump can be quantified using gliders (pink instruments) and subsequent modelling³¹, BGC-Argo floats (bio-optics/oxygen/physics)⁹³ or surveys based on multiple POC profiles in conjunction with coupled models (regional circulation/particle dynamics)^{30,49}. e) quantification of the mesopelagic migrant pump (active diel transport of carbon by mid-water biota, denoted by moon and sun symbols) requires mid-water trawl surveys along with metabolic modelling^{54,55}. Some multidisciplinary studies^{30,31,49} have combined these approaches to cross-compare export flux from the BGP (green arrows (d)) and the eddy subduction pump (purple arrows represent subsurface particle maxima recorded at the eddy periphery³¹). Note, the large-scale subduction pump²³ is not presented here.

